Enhancement and Suppression of Resonance Energy Transfer Near Metal Nanoparticles

Yeonjun Jeong[†] *and George C. Schatz*[*, †, ‡]

[†]Department of Chemistry and [‡]Graduate Program in Applied Physics, Northwestern University, Evanston, Illinois 60208, United States

ABSTRACT

Plasmons are known to promote light-matter interaction, providing a powerful tool to increase the rate of energy transfer between donor and acceptor molecules that are appropriately located near a plasmonic particle, a phenomenon called plasmon-coupled resonance energy transfer (PC-RET). In this work, we utilize a Mie theory-based method to calculate the PC-RET rate for a donor-acceptor pair interacting with a single spherical particle, with the goal of identifying key geometrical factors in plasmonic systems that determine the RET rate. We also determine the plasmon enhancement contribution to absorption by the donor, and then combine this with RET efficiency to determine plasmon enhancement to the overall acceptor formation rate. We find that RET is often suppressed by coupling to plasmons on a single-molecule level although plasmon-enhanced absorption can lead to a net increase in acceptor formation rate in the presence of the nanoparticle. A quasistatic analysis reveals the dependence of multipolar contributions on the distance of the fluorophores from the metal particle. Finally, it is demonstrated from an analysis

of experimental RET results that the structure of a nanophotonic system can be determined from sensitivity of RET rate to the system geometry.

INTRODUCTION

Plasmons are a collective oscillation of the conduction electrons in metals when irradiated with electromagnetic (EM) waves. In the last 50 years, applications involving plasmons have rapidly evolved thanks to improvement in nanofabrication techniques, both in lithography (top-down) and synthesis (bottom-up).[1-2] The ability of plasmons to efficiently couple to the far-field has led to such diverse applications as new lasing technologies[3] and biomarkers for cancer cells[4-5]. Nonradiative decay of plasmons leads to local heating, which is useful for tumor destruction[6]. Another group of applications stems from the interaction of molecules with the strong EM field near the plasmonic nanoparticles (NPs), which can promote chemical reactions or enhanced sensitivity in sensing applications[7-23]. Resonance energy transfer (RET) coupled to plasmons, which we denote plasmon-coupled resonance energy transfer (PC-RET), falls into the last category, and it is sometimes observed that the RET rate can be enhanced near plasmonic NPs due to modification of the photonic mode density.[17, 22, 24] For example, Wenger and coworkers have achieved enhancement of the RET rate at the single-molecule level by employing various structures such as a gold[19] and silver[21] nanoaperture, an aluminum nanoantenna,[25-26] a gold dimer cavity[18], and a silver nanowire[27]. Bradley and coworkers have used a structure where a layer of gold NPs was sandwiched by a donor and acceptor quantum dot layer to determine the distance dependence of the RET rate, including results that were still observable out to 20 nm separation.[28] In work by Bujak et al., the donor and the acceptor molecules were attached to the tip of a gold nanorod, and RET enhancement could be switched on and off by changing polarization of the

excitation light.[29] PC-RET was also achieved by Bohlen et al. and by Anderson et al. using DNA origami to precisely control where the donor, acceptor and nanoparticle are located.[30-31]

The theory of RET between two point electric dipoles under the electrostatic approximation in a non-absorbing, non-dispersing homogeneous space is known as Förster theory. The rate expression reads[32-33]

$$\gamma_{RET} = \frac{\Phi_D}{\tau_D}\frac{9000(\ln 10)\kappa^2}{128\pi^5 N_A n_r^4 R^6}\int d\bar{\nu}\,\frac{\epsilon_A(\bar{\nu})I_D(\bar{\nu})}{\bar{\nu}^4} \text{ (Gaussian Units),}$$

$$= \frac{\Phi_D}{\tau_D}\frac{9c^4\kappa^2}{8\pi n_r^4 R^6}\int d\omega\,\frac{\sigma_A(\omega)I_D(\omega)}{\omega^4} \text{ (SI Units)} \quad (1)$$

where Φ_D and τ_D are the intrinsic fluorescence quantum yield (QY) and decay lifetime of the donor molecule (in the medium where the emission spectrum is obtained), respectively, κ^2 is the orientation factor defined by the orientations of the geometry of the two dipoles, N_A is Avogadro's number, n_r is the refractive index of the medium, R is the distance between the donor and the acceptor, $\bar{\nu}$ is the wavenumber, $\epsilon_A(\bar{\nu})$ is the molar absorptivity of the acceptor (in $L \cdot mol^{-1} \cdot cm^{-1}$), ω is the frequency, $\sigma_A(\omega)$ is the absorption cross-section of the acceptor (in m^2), and $I_D(\bar{\nu})$ is the area-normalized emission spectrum of the donor.

Intermediate and far zone interactions become increasingly important for distances much beyond 10 nm, and also, plasmonic or photonic structures can modify the RET rate, requiring a more general formula. Theoretical studies have pursued both formalisms based on classical[24, 34] (CED) and quantum electrodynamics[35-44] (QED), and a thorough review has been published.[45] The rate expression in a general dielectric environment has been derived based on a Green tensor formalism,[46-47] which reads in SI units

$$\gamma_{RET} = \frac{18\pi\Phi_D}{\mu_0^2\tau_D}\int_0^\infty d\omega\,\left|\boldsymbol{e}_A \cdot \overleftrightarrow{G}(\boldsymbol{r}_A, \boldsymbol{r}_D; \omega) \cdot \boldsymbol{e}_D\right|^2 \sigma_A(\omega)I_D(\omega), \quad (2)$$

where μ_0 is the vacuum permeability, ω is the angular frequency, $\boldsymbol{e}_D$ and $\boldsymbol{e}_A$ are the normalized transition dipole moments of the donor and the acceptor, respectively, and $\boldsymbol{r}_D$ and $\boldsymbol{r}_A$ are the positions of the donor and the acceptor, respectively. $\overleftrightarrow{G}(\boldsymbol{r}, \boldsymbol{r}'; \omega)$ is a Green tensor defined as the solution of

$$\nabla \times \nabla \times \overleftrightarrow{G}(\boldsymbol{r}, \boldsymbol{r}'; \omega) - \frac{\omega^2}{c^2}\epsilon(\boldsymbol{r}, \omega)\overleftrightarrow{G}(\boldsymbol{r}, \boldsymbol{r}'; \omega) = \overleftrightarrow{I}\,\delta(\boldsymbol{r} - \boldsymbol{r}'), \quad (3)$$

where c is the speed of light in vacuum, $\overleftrightarrow{I}$ is the unit dyad, and $\delta(\boldsymbol{r} - \boldsymbol{r}')$ is the Dirac delta function. In practice, it is difficult to calculate $\overleftrightarrow{G}(\boldsymbol{r}_A, \boldsymbol{r}_D; \omega)$ in a complex, nonhomogeneous dielectric environment. To overcome this, Maxwell's equations can be used to transform Eq. (3) to

$$\gamma_{RET} = \frac{\Phi_D}{\tau_D}\frac{18\pi}{\mu_0^2}\int d\omega \frac{1}{\omega^4}\frac{\left|\boldsymbol{e}_A \cdot \boldsymbol{E}_D^{tot}(\boldsymbol{r}_A, \omega)\right|^2}{|\boldsymbol{p}_D|^2}\,\sigma_A(\omega) I_D(\omega), \quad (4)$$

so that the electric field from the donor $\boldsymbol{E}_D^{tot}(\boldsymbol{r}_A, \omega)$, including the response of the environment, is used to obtain the RET rate.[48-49] Here, $\boldsymbol{p}_D$ is the magnitude of the donor electric dipole used in a CED simulation to obtain $\boldsymbol{E}_D^{tot}(\boldsymbol{r}_A, \omega)$. This formalism highlights the bridging between QED and CED in that the interaction between the transition dipoles is described by a classical Green tensor. Here, the RET rate is governed by not only by the spectral overlap of the donor emission and the acceptor absorption but also by the EM coupling of the two dipoles, leading to the generalized spectral overlap (GSO) defined in the integral in Eq. (4). In particular, the EM coupling can be modified by plasmon excitation in a nearby NP, which changes GSO integrand.[49] A similar concept has been proposed for fluorescence emission by Feldmann and coworkers[50].

Eq. (4) provides a convenient way to study PC-RET. For example, Schatz and coworkers have demonstrated that the RET enhancement spectrum of a metal NP can be fundamentally different

from the extinction spectrum of that NP.[49] A further investigation showed that the dominant localized surface plasmon (LSP) modes in RET vary with the particle size, and often involve high multipole plasmons that are unimportant in other optical properties such as extinction spectra.[51] . A related phenomenon shows up concerning strong coupling effects in emitters that are coupled to plasmonic particles.[52] Eq. (4) has also been applied to a flat metal surface to characterize the effect of a mirror dipole, SPP, and retardation to RET.[53]

It should be noted that the local field factor $\left(\frac{\epsilon_b+2}{3}\right)^2$ obtained by explicitly coupling the electric displacement field operator to the dipole moment operators of bath molecules as well as to the donor and acceptor,[43] where ϵ_b is the dielectric constant of the background medium, is not included in Eq. (4). Also, the coupling factor $M^{p-p} \equiv \boldsymbol{e}_A \cdot \overleftrightarrow{G}(\boldsymbol{r}_A, \boldsymbol{r}_D; \omega) \cdot \boldsymbol{e}_D$ concerns only electric dipoles, but higher-order multipoles may become important when the donor–acceptor (D-A) distance is small enough to be comparable to the size of the fluorophores.[54] Furthermore, the electric dipole–magnetic dipole interaction M^{p-m} may dominate when the dipoles and the intermolecular vector form a orthogonal triad,[37, 54] and the magnetic dipole–magnetic dipole interaction M^{m-m} may couple significantly to M^{p-p}.[55]

In PC-RET, the rate strongly depends on the size of the NP, and on the positions and orientations of the donor and acceptor with respect to the NP. Theoretical investigation of RET as a function of the geometry of the system is therefore important since ensemble measurements can obscure pronounced effects that may arise for individual geometries. In this work, we consider a system of a donor electric dipole, an acceptor electric dipole, and a metal (gold or silver) sphere to examine the conditions that lead to enhancement of the RET rate, and in particular, to show how RET rate can be suppressed relative to that in the absence of a nanoparticle for a wide range of geometries.

We also examine the effect of plasmon enhanced absorption by the donor in combination with RET to determine the overall rate of acceptor formation (AF), showing that the AF rate (relevant to further processes such as acceptor fluorescence, RET to another molecule, absorption of energy by the metal, intramolecular decay, and chemical reaction) follows a similar trend to RET although AF may be enhanced even when RET is suppressed. We further provide new physical insights concerning the contribution of plasmon multipoles to RET using a quasistatic analysis. Finally, by analyzing a recent experiment, it is demonstrated that the sensitivity of RET rate to the geometry of the system can be used to provide important structural information on the donor-acceptor-nanoparticle system.

THEORY

The influence of a plasmonic nanostructure on RET rate can be quantified by the frequency-specific plasmon enhancement factor (PEF) defined as

$$PEF(\omega) = \frac{\left|\boldsymbol{e}_A^* \cdot \boldsymbol{E}_D^{tot}(\boldsymbol{r}_A,\omega)\right|^2}{\left|\boldsymbol{e}_A^* \cdot \boldsymbol{E}_D^{inc}(\boldsymbol{r}_A,\omega)\right|^2}. \quad (5)$$

Here, $\boldsymbol{E}_D^{tot} = \boldsymbol{E}_D^{inc} + \boldsymbol{E}_D^{sca}$, where $\boldsymbol{E}_D^{inc}$ is the direct incident field from the donor dipole and $\boldsymbol{E}_D^{sca}$ is the scattered field from the nanostructure. $\boldsymbol{E}_D^{inc}$ is readily obtainable,[56] and Mie theory[57-59] provides the exact $\boldsymbol{E}_D^{sca}$ from homogeneous spheres given that the fields are expanded to a sufficiently high order. We consider the donor at $\boldsymbol{r}'$ and the acceptor at $\boldsymbol{r}$, both outside of the sphere, of which the radius is a and the center is set as the origin. Then, the incident and scattered electric field are expanded as

$$\boldsymbol{E}_D^{inc}(\boldsymbol{r}) = \sum_{lm}\left[u_{lm}\boldsymbol{N}_{lm}^{(1)}(k_b,\boldsymbol{r}) + v_{lm}\boldsymbol{M}_{lm}^{(1)}(k_b,\boldsymbol{r})\right] \ (a < r < r') \ (6)$$

$$\boldsymbol{E}_D^{sca}(\boldsymbol{r}) = \sum_{lm}\left[a_{lm}\boldsymbol{N}_{lm}^{(3)}(k_b,\boldsymbol{r}) + b_{lm}\boldsymbol{M}_{lm}^{(3)}(k_b,\boldsymbol{r})\right] \ (r > a). \ (7)$$

The frequency dependence is omitted for brevity. Here, $k_b = \frac{\omega}{c}\sqrt{\epsilon_b}$, where ϵ_b is the dielectric function of the background medium. The basis functions $\boldsymbol{N}_{lm}^{(1)}$, $\boldsymbol{M}_{lm}^{(1)}$, $\boldsymbol{N}_{lm}^{(3)}$, $\boldsymbol{M}_{lm}^{(3)}$ ($l = 0, 1, 2, \ldots$ and $m = -l, -l+1, \ldots, 0, \ldots, l-1, l$), are the vector spherical harmonics (VSH), defined as

$$\boldsymbol{M}_{lm}^{(i)}(k,\boldsymbol{r}) = \frac{1}{\sqrt{l(l+1)}}\nabla \times \left(\boldsymbol{r} z_l^{(i)}(kr) Y_{lm}(\theta,\phi)\right) \ (8)$$

$$\boldsymbol{N}_{lm}^{(i)}(k,\boldsymbol{r}) = \frac{1}{k}\nabla \times \boldsymbol{M}_{lm}^{(i)}(k,\boldsymbol{r}). \ (9)$$

Here $z_l^{(1)}$and $z_l^{(2)}$ ($z_l^{(3)}$and $z_l^{(4)}$) are spherical Bessel (Hankel) functions of the first and second kind, respectively, and $Y_{lm}(\theta,\phi) = \sqrt{\frac{2l+1}{4\pi}\frac{(l-m)!}{(l+m)!}}P_l^m(cos\theta)e^{im\phi}$ are the spherical harmonics, where the associated Legendre function P_l^m is defined as $P_l^m(x) = \frac{(-1)^m}{2^l n!}(1-x^2)^{\frac{m}{2}}\frac{d^{l+m}}{dx^{l+m}}(x^2-1)^l$ and $P_l^{(-m)}(x) = (-1)^m\frac{(l-m)!}{(l+m)!}P_l^m(x)$ for $m \geq 0$. The incident coefficients for a point dipole source and a single sphere are (in SI units)[60-61]

$$u_{lm} = (-1)^m\left(i\frac{k_b^3}{\epsilon_0\epsilon_b}\right)\boldsymbol{N}_{l(-m)}^{(3)}(k_b,\boldsymbol{r}')\cdot\boldsymbol{p}_D \ (10)$$

$$v_{lm} = (-1)^m\left(i\frac{k_b^3}{\epsilon_0\epsilon_b}\right)\boldsymbol{M}_{l(-m)}^{(3)}(k_b,\boldsymbol{r}')\cdot\boldsymbol{p}_D, \ (11)$$

and the scattering coefficients are related by

$$a_{lm} = \frac{\psi_l(x)\psi_l'(sx) - s\psi_l(sx)\psi_l\prime(x)}{s\psi_l(sx)\xi_l'(x) - \xi_l(x)\psi_l\prime(sx)}u_{lm} \ (12)$$

$$b_{lm} = \frac{s\psi_l(x)\psi_l'(sx) - \psi_l(sx)\psi_l\prime(x)}{\psi_l(sx)\xi_l'(x) - s\xi_l(x)\psi_l\prime(sx)} v_{lm}, \quad (13)$$

where $\psi_l(x)$ and $\xi_l(x)$ are the Riccati–Bessel functions, defined as $\psi_l(x) = xz^{(1)}(x)$ and $\xi_l(x) = xz^{(3)}(x)$, and the prime denotes derivate. Also, $x = k_b a$ and $s = \sqrt{\frac{\epsilon_m}{\epsilon_b}}$, where ϵ_m and ϵ_b stand for the permittivity of the sphere and the background medium, respectively. For multiple spheres, the scattering coefficients of each sphere are coupled, forming a system of equations.[62-63] $\boldsymbol{E}_D^{tot}(\boldsymbol{r}_A, \omega)$ is obtained by summing up $\boldsymbol{E}^{inc}(\boldsymbol{r}_A, \omega)$ and $\boldsymbol{E}^{sca}(\boldsymbol{r}_A, \omega)$ and then plugged into Eq. (4) to obtain the RET rate.

Despite its conceptual simplicity, Mie theory provides little physical insight because the electric fields are expressed in complex vectorial functions. This can be avoided in the quasistatic limit, where the electric field is derived from the electric potential, which has a simple scalar expression. Gauss's law states

$$\nabla \cdot \boldsymbol{D}(\boldsymbol{r}, \omega) = \rho_s(\boldsymbol{r}, \omega), \quad (14)$$

where $\boldsymbol{D}(\boldsymbol{r}, \omega) = \epsilon_0 \epsilon(\boldsymbol{r}, \omega)\boldsymbol{E}(\boldsymbol{r}, \omega)$ is the electric displacement, $\rho_s(\boldsymbol{r}, \omega)$ is the source charge distribution, and $\epsilon(\boldsymbol{r}, \omega)$ is the relative permittivity. This is equivalent to Poisson's equation

$$-\nabla \cdot \epsilon(\boldsymbol{r}, \omega)\nabla\Phi(\boldsymbol{r}, \omega) = \frac{\rho_s(\boldsymbol{r},\omega)}{\epsilon_0}, \quad (15)$$

where the electric potential $\Phi(\boldsymbol{r}, \omega) = -\nabla \boldsymbol{E}(\boldsymbol{r}, \omega)$ is introduced. Here, the del operators designate derivatives with respect to the position vector $\boldsymbol{r}$. In the case of a single sphere, $\epsilon(\boldsymbol{r}, \omega) = \Theta(a - r)\epsilon_m + \big(1 - \Theta(a - r)\big)\epsilon_b$, where Θ is the Heaviside step function. To solve this equation, we first define the scalar Green function $g^{tot}(\boldsymbol{r}, \boldsymbol{r}'; \omega)$ using

$$-\nabla \cdot \epsilon(\boldsymbol{r},\omega)\nabla g^{tot}(\boldsymbol{r},\boldsymbol{r}';\omega) = \delta(\boldsymbol{r}-\boldsymbol{r}'). \quad (16)$$

Solving Eq. (16) assuming that the source (donor) and the acceptor are outside the sphere (i.e. $r' > a$ and $r > a$) gives[64]

$$g^{tot}(\boldsymbol{r},\boldsymbol{r}';\omega) = g^{inc}(\boldsymbol{r},\boldsymbol{r}') + g^{sca}(\boldsymbol{r},\boldsymbol{r}';\omega), \quad (17)$$

where

$$g^{inc}(\boldsymbol{r},\boldsymbol{r}') = \frac{1}{4\pi\epsilon_b|\boldsymbol{r}-\boldsymbol{r}'|} \quad (18)$$

$$g^{sca}(\boldsymbol{r},\boldsymbol{r}';\omega) = -\sum_{l=1}^{\infty}\sum_{m=-l}^{l}\frac{1}{2l+1}\frac{1}{\epsilon_b}\frac{l(\epsilon_m/\epsilon_b-1)}{l(\epsilon_m/\epsilon_b+1)+1}\frac{a^{2l+1}}{r'^{l+1}r^{l+1}}Y_{lm}(\theta,\phi)Y_{lm}^{*}(\theta',\phi'). \quad (19)$$

g^{inc} corresponds to the potential originating directly from the point source $\delta(\boldsymbol{r}-\boldsymbol{r}')$ and g^{sca} reflects the scattering by the sphere. For convenience, each multipolar contribution to the scattering term is defined as

$$g_{lm}^{sca}(\boldsymbol{r},\boldsymbol{r}';\omega) = -\frac{1}{2l+1}\frac{1}{\epsilon_b}\frac{l\left(\frac{\epsilon_m}{\epsilon_b}-1\right)}{l\left(\frac{\epsilon_m}{\epsilon_b}+1\right)+1}\frac{a^{2l+1}}{r'^{l+1}r^{l+1}}Y_{lm}(\theta,\phi)Y_{lm}^{*}(\theta',\phi'). \quad (20)$$

g_{lm}^{sca} are independent of the kind of the source charge and therefore encodes the intrinsic properties of the LSPs. The factor $\frac{l(\epsilon_m/\epsilon_b-1)}{l(\epsilon_m/\epsilon_b+1)+1}$ determines the resonance wavelength for each l, and $\frac{a^{2l+1}}{r'^{l+1}r^{l+1}}$ shows the relative contribution of each multipole on the geometry of the system. The latter is more clearly seen by using the relation $\boldsymbol{E}_D(\boldsymbol{r},\omega) = -\frac{1}{\epsilon_0}\nabla_{\boldsymbol{r}}\left(\boldsymbol{p}_D \cdot \left(\nabla_{\boldsymbol{r}'}g(\boldsymbol{r},\boldsymbol{r}';\omega)\right)_{\boldsymbol{r}'=\boldsymbol{r}_D}\right)$,[65] which leads to the contribution of each multipole to the scattered field $\boldsymbol{E}_{D,lm}^{sca}(\boldsymbol{r},\omega) \propto \frac{a^{2l+1}}{r_D^{l+2}r_A^{l+2}} = \frac{1}{a}\left(\frac{a}{r_D}\right)^{l+2}\left(\frac{a}{r_A}\right)^{l+2}$.

When $\frac{a}{r_D} \ll 1$ and $\frac{a}{r_A} \ll 1$ (i.e. when the sphere is relatively small compared to the fluorophore–sphere surface distances), $\boldsymbol{E}_{D,lm}^{sca}$ decays rapidly with increasing l. Thus, higher-order multipole contributions to the scattered field are small. Conversely, if the fluorophores are in the proximity to the sphere surface, many higher order multipoles participate in RET (or any other processes involving the scattered field).

A more complete picture of the excited acceptor formation rate involves combining the absorption of energy (e.g. from an external field) by the donor and the competition between RET and other donor decay processes, namely absorption by the NP, radiation to the far-zone, and intramolecular nonradiative decay. AF rate can thus be written as

$$\gamma_{AF} = \gamma_{D,abs} \times q_{RET}, \quad (21)$$

where $\gamma_{D,abs}$ is the donor absorption rate and $q_{RET} = \frac{\gamma_{RET}/\gamma_r^0}{\gamma_{RET}/\gamma_r^0 + \gamma_{abs}/\gamma_r^0 + \gamma_r/\gamma_r^0 + (1-q^0)/q^0}$ is the QY for the RET process. Here, $q^0, \gamma_r^0, \gamma_r$ and γ_{abs} are, respectively, the intrinsic fluorescence QY of the donor in the absence of the nanoparticle (usually obtained from experiment), the intrinsic fluorescence rate of the donor, the radiation rate in the presence of the nanoparticle (to the far zone), and the absorption rate by the NP. The last term in the denominator of q_{RET}, when multiplied by γ^0, represents rate of intramolecular nonradiative decay. To see the influence of the nanostructure, the ratio of AF rates with and without the NP (leaving the donor and the acceptor at the same position) is calculated at single wavelength by taking $\gamma_{D,abs} \propto |\boldsymbol{p}_D \cdot \boldsymbol{E}_{PW}(\boldsymbol{r}_D, \omega)|^2$,[66] where $\boldsymbol{E}_{PW}$ is the electric field generated by an external plane wave (which may be modified by the NP), and calculating γ_{RET} with Eq. (4). Also, $\gamma_{D,abs} + \gamma_r = \frac{2}{\hbar} Im\big(\boldsymbol{p}_D \cdot Im\, \boldsymbol{E}_D(\boldsymbol{r}_D, \omega)\big)$,[24, 46] and q^0 is taken to be 1 in the evaluation presented later. We should note that if a further process (such

as acceptor fluorescence) is of interest, then the quantum yield of that process should also be factored in. This will not be included in our analysis.

RESULTS AND DISCUSSION

All of the analysis except for our study of an experiment in section (e) below will consider a D-A combination in the presence of a single spherical gold or silver NP with the donor and acceptor at various locations (as defined by the angle associated with the donor, the sphere center, and the acceptor and the distance from the NP surface). The analysis will first consider PC-RET, and then we include donor absorption and RET efficiency to determine the AF enhancement.

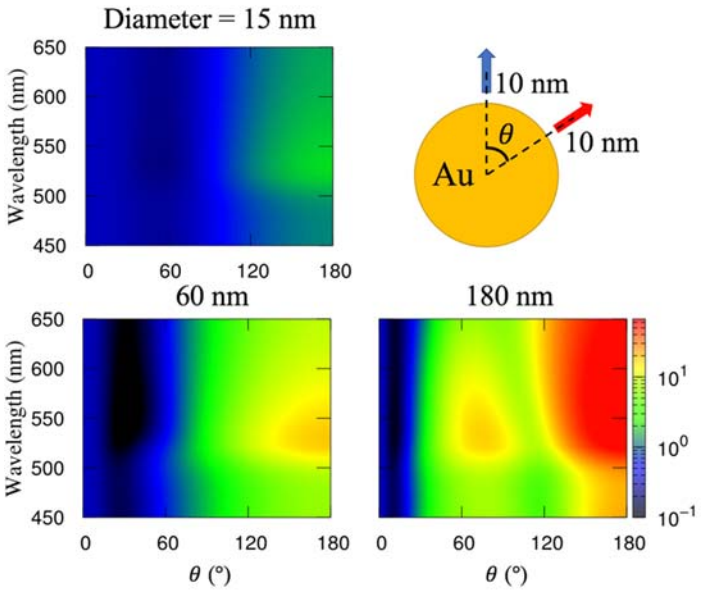

Figure 1. RET enhancement spectrum as a function of the wavelength of photon being transferred and the angle defined by donor–sphere center–acceptor as calculated using Mie theory. The dipole–sphere surface separation was kept at 10 nm. The background medium was vacuum.

a) Effect of Particle Size.

First, the particle size and the angle are taken as variables, the dipole-surface separation is fixed at 10 nm, and the dipole directions are set to be perpendicular to the metal (gold or silver) surface. The PEF is calculated using Mie theory for three different particle sizes as a function of the angle and wavelength (Figure 1). Regardless of the particle size, diametrically located dipoles ($\theta = 180°$) produce the maximum enhancement, and larger spheres lead to larger enhancement at that relative position. A similar trend is observed with

a silver sphere (Figure S1). However, it should be noted that a higher PEF does not mean a higher RET rate. As the particle size grows, the D-A distance increases, leading to a smaller RET rate. Nevertheless, this demonstrates that large NPs are effective in promoting long-distance RET. Later we will also factor in the effect of donor absorption enhancement, as this ultimately determines the rate of acceptor formation.

Interestingly, there is a range of angles where RET is suppressed in the presence of the NP (for gold, throughout the entire range of wavelengths investigated, and for silver, wavelengths over 355 nm), appearing as the blue to black in Figure 1 and Figure S1. This occurs because of destructive interference of the direct electric field from the dipole and the scattered field from the particle.[51] Note that the very pronounced suppression observed for a silver sphere around a wavelength of 325 nm is because there are no surface plasmons at that wavelength, and bulk plasmon excitation is ineffective as there is too much extinction in penetrating through the particle.[51]

b) Effect of Fluorophore Geometry.

Fluorophores attached to a NP are often oriented randomly or with a wide range of orientations, so it is important to study the effect different orientations on the results. Figure 2 illustrates the PEF profile as a function of the angle θ for various gold sphere sizes and three different orientations of the dipoles (one radial and two tangential to the NP surface), at the wavelength of 540 nm, where the plasmonic response of the gold NPs is strong. It is readily noticeable that the PEF is mostly below 1 for the tangential systems. Also, PEF for the radial case is smaller than 1 at some small angles, as mentioned above. For a silver sphere, both strong suppression and enhancement are observed in all three orientation setups, featuring a transition from suppression to enhancement with increasing angle (Figure S3).

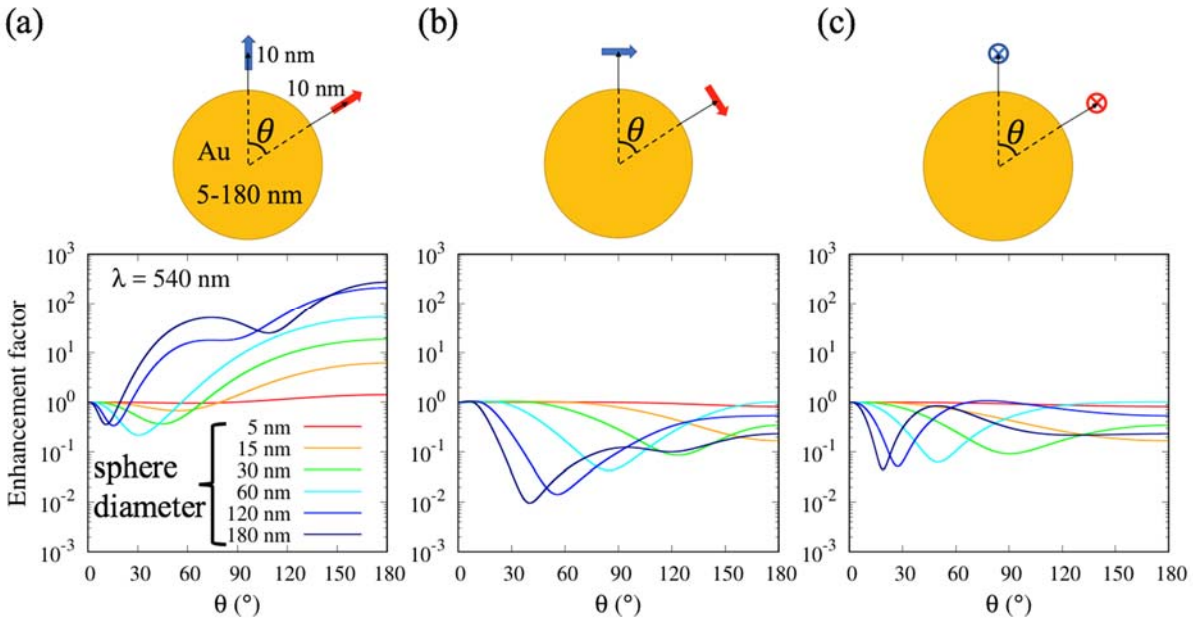

Figure 2. Enhancement factor of RET at 540 nm calculated with a gold sphere of varying size using Mie theory in three different orientations versus the position of the acceptor dipole represented as the angle between the donor and the acceptor dipole. The background medium was vacuum.

Another important parameter in determining the system geometry is the separation distance of the dipoles from the surface of the particle. Figure 3 shows the PEF at a wavelength of 540 nm for a gold particle of 60 nm-diameter and the two dipoles located at various relative positions (separation distances 1-100 nm, and angles 30° to 180°). As the dipoles get closer to the metal

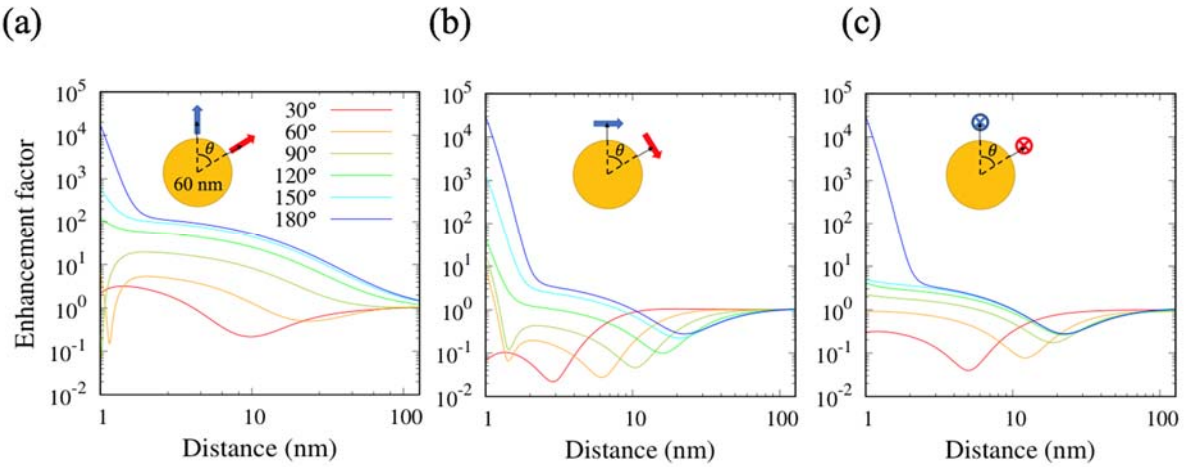

Figure 3. The dependence of the enhancement factor on the distance between the dipoles and the metal (gold) surface at various relative positions of the dipoles for three different dipole orientations. The donor and acceptor are equally separated from the surface, and the diameter of the sphere is 60 nm. The background medium was vacuum.

surface, for the radially oriented dipoles, the PEF increases monotonically for larger angles (120° to 180°) and suppression occurs for smaller angles (30° to 90°). When the dipoles are tangentially oriented, the PEF show a minimum at 2-20 nm, and then goes up for smaller distances, usually giving a large enhancement near 1 nm (with the exception of 30°, where the PEF stays below 1). A silver sphere gives a similar result despite minor differences in whether the PEF drops below 1 at small angles in the radial orientation and if it stays below 1 for 30° in the tangential orientation (Figure S5). Generally, the dipoles at the opposite sides of the NP and close to the surface give the largest PEF, and radially oriented dipoles are preferred over tangential ones to generate net RET enhancement.

We conclude that RET can be suppressed for both gold and silver and for a wide range of dipole locations and orientations. This conclusion is in apparent contrast to the observations of enhancements in many experiments.[18-19, 21, 25-29] However, there are many reasons why this discrepancy might not be real, including issues with unknown fluorophore orientations or unknown D-A separations. Also, an extremely large RET enhancement for certain geometries can

compensate for suppression in other geometries, resulting in the overall apparent enhancement. This may occur when special positions and orientations of fluorophores are possible or when the NPs are densely coated with fluorophores. It is interesting to note that apart from the geometry effect, a dependence of RET rate on particle coverage (with fluorophores) can appear due to coupling among the fluorophore excitons and the plasmons, similar to the dependence of surface-enhanced resonance Raman spectroscopy (SERRS) signal on the coverage.[67] The effect of enhanced donor absorption on the result can also influence the experiments as we discuss later.

Interestingly, for the radial system and a fixed dipole–surface separation, the length of the arc formed by the D-A pair around the sphere at the minimum PEF is surprisingly consistent (20 nm for the separation of 10 nm) throughout various particle sizes and wavelengths, especially for gold (Figure S4). This critical distance is observed to grow as the dipole–NP separation increases. However, for a limited range of fluorophore–NP separations, as could arise in the scenario where the fluorophores are attached to the metal surface by a linker, this distance can be used as an indicator of the RET suppression region.

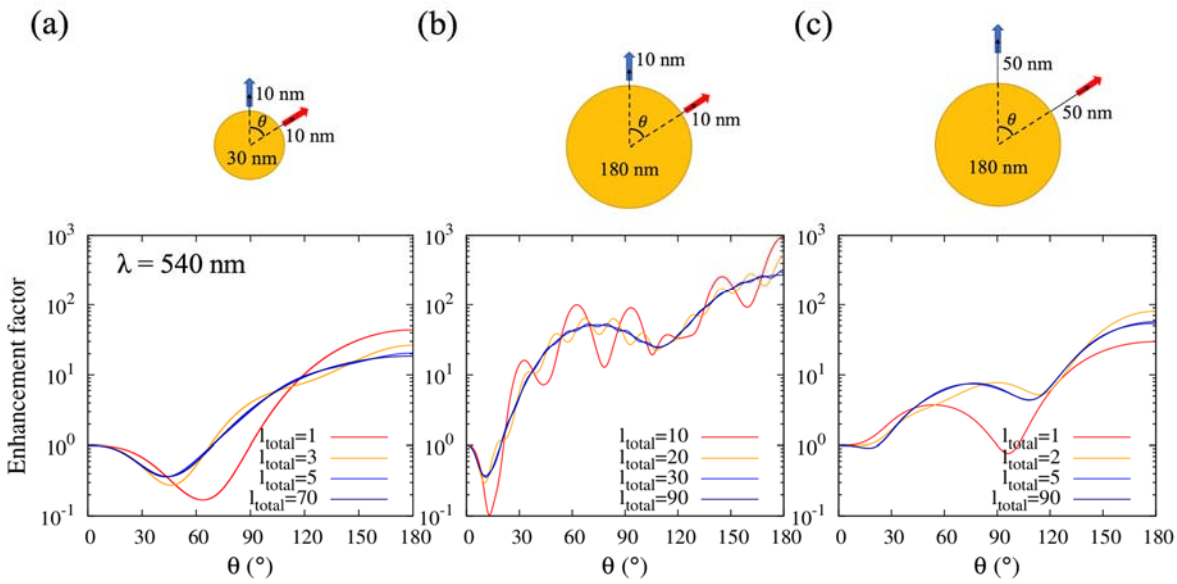

Figure 4. RET enhancement factor in a system consisting of a gold sphere and radially oriented donor and acceptor dipole, with varying sphere diameter and dipole-surface separation, calculated using Mie theory up to the specified orders. The enhancement factor is plotted against the angle defined by the donor, the center of the sphere, and the acceptor. l_{total} stands for the number of modes included in the calculation (e.g. l_{total}=3 includes dipole, quadrupole, and octopole). Wavelength was fixed at 540 nm, and the background medium was vacuum.

c) Analysis of Multipole Contributions.

Eq. (20) predicts that higher-order multipole modes participate more in RET for fluorophore separations from the NP surface that are relatively small compared to the sphere radius. Figure 4 demonstrates this using Mie theory. Comparing Figure 4(a) and 4(b), for the same dipole-metal separation distance, while only 5 multipoles are needed to successfully approximate the exact PEF profile ($l_{total} = 70$) for a 30-nm diameter sphere, at least 30 multipoles are needed to accurately describe the exact result ($l_{total} = 90$) for a 180-nm diameter sphere. The comparison of Figure 4(b) and 4(c) shows that with a larger separation from the metal surface, a smaller number of multipoles are needed. A similar argument on the particle size and fluorophore–sphere separations is possible beyond the electric dipole approximation due to the source independence of g_{lm}^{sca} in Eq. (20).

This analysis highlights the fundamental difference between the importance of multipole contributions for plane wave excitation and PC-RET. In PC-RET, contributions of higher-order multipoles vary significantly depending on not only the particle size but also the positions of the molecules, and very high order multipoles may be important if the fluorophores are very close to the NP surface. For example, while plasmon excitation of a spherical NP of diameter up to tens of nanometers by a plane wave can be well approximated by an induced dipole or quadrupole[51, 68], at least up to the $l = 5$ modes are needed to correctly describe PEF for a 30-nm diameter gold sphere and the dipoles separated by 10 nm from the sphere surface.

While the quasistatic approximation gives useful physical insights, it does not accurately describe the electric field for large particles and distances (roughly larger than 30 nm). Slightly better agreement with the exact result can be achieved by applying correction factors to calculate the induced dipole and quadrupole moments of the NP and then using the fully-retarded electric fields.[65]

d) Inclusion of Plasmon-Enhanced Absorption.

As formation rate of the acceptor involves absorption by the donor and competing processes to RET (absorption by NP, radiation, and intramolecular decay), the AF rate as a function of geometry is expected to be different from that of RET. However, it is important to note that the processes

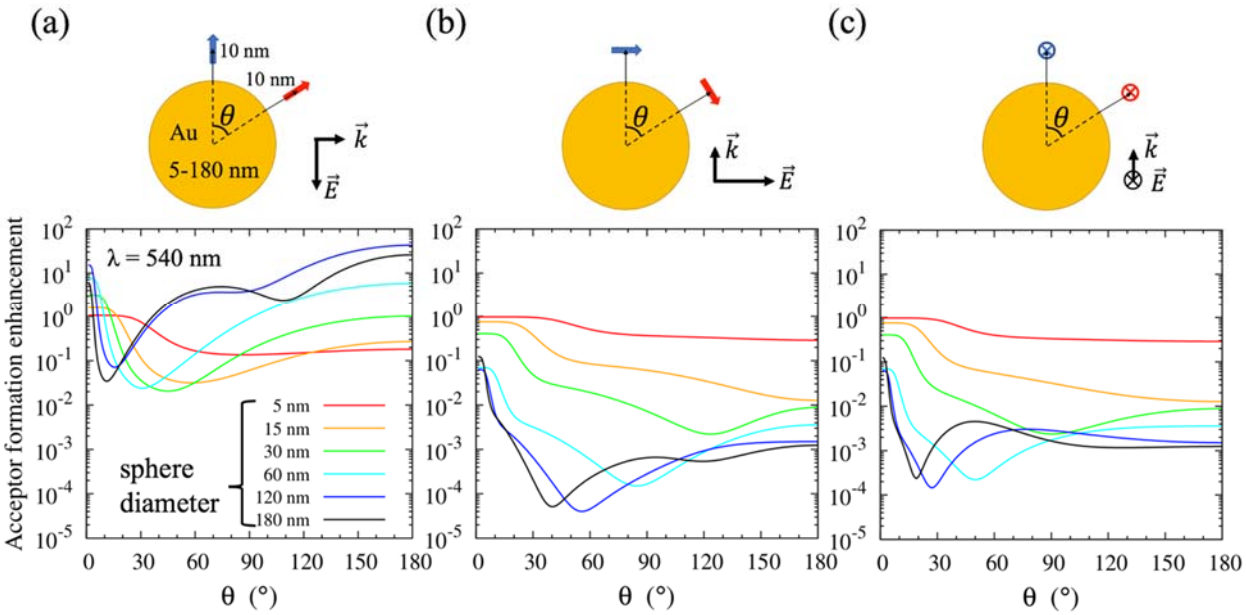

Figure 5. Acceptor formation enhancement factor plotted versus the angle formed by the donor, the sphere center, and the acceptor for various sphere sizes. The wavevector and the polarization vector of the exciting plane wave are shown as black arrows. The acceptor absorption lineshape was modeled as a Gaussian function with the peak at 540 nm and the full width at half maximum (FWHM) of 60 nm, and the donor emission lineshape was taken to be a Dirac delta function at 540 nm. The background medium was vacuum.

other than RET only involve the donor and the NP. As a result, the effect of these processes is constant as acceptor geometry is changed. Figure 5 illustrates the AF enhancement factor using the same systems as in Figure 2, where the RET enhancement factor is plotted. Similar to RET, AF shows enhancement for radial dipole orientations (Figure 5(a)) and is suppressed for tangential dipoles (Figure 5(b) and 5(c)). The suppression region in Fig. 2 for the radial system is also present in the AF, but the particle needs to be large enough (≥ 60 nm diameter) for AF enhancement to occur at large angles. At small angles, since the RET QY is close to 1, the AF enhancement converges to the donor absorption enhancement factor. Note that donor absorption enhancement occurs for radial donor dipole orientations and suppression appears in the tangential orientation, a tendency also appearing in RET enhancement (Table S1).

e) Application of RET Theory to an Experimental System.

Here, we examine the single-molecule RET experiment of Bidault et al.[18], focusing on the influence of the geometry of the plasmonic system, wherein each single D-A pair was linked to the center of a DNA strand of length 14 nm and two gold spheres of equal size (40 or 60 nm in diameter) were attached to each end of the DNA. In this work, the D-A separation was estimated to be 4 ± 1 nm, taking into account the molecular linkers that connect the dyes to the DNA bases. The interparticle gap distance was measured to be 14 ± 2 nm using cryoelectron microscopy, meaning that there was little bending of DNA in that measurement. However, in solutions in room temperature, where the RET measurements were performed, the DNA strand may bend to bring the spheres closer due to the flexible linker attachments to the gold particle. Also, although DNA is a relatively stiff polymer, with a persistence length of ~50 nm in 0.1 M aqueous NaCl, the ionic environment can modify the phosphate-phosphate repulsion in the DNA backbone.[69] To study this system, various possible geometries were modeled (See Figure S5) and the resulting simulated RET rates with orientation averaging of the dipole directions and including the local field factor mentioned above were tabulated (Table 1). The D-A separation distance was set to 5 nm as this distance makes the orientation-averaged rate without NP as calculated with Eq. (1) close to the experimental value. It is seen that in the case of the vertically positioned fluorophores (D-A axis perpendicular to the interparticle axis, see Figure S5) and a 14-nm gap (without DNA bending), the simulated RET rate with the NPs is much smaller than the experimental value. A value similar to the experiment can be achieved with the fluorophores deviating from the vertical position and with a smaller interparticle gap (horizontal, 10 nm or diagonal, 4 nm). This indicates that the DNA strand attachment at the gold nanoparticle is bent to produce a smaller interparticle gap than 14 nm leading to fluorophores that are closer to the NPs. While there is a range of possible gaps and orientations that are consistent with the experimental results, this demonstrates that the sensitivity

of the RET rate with respect to the system geometry is useful in determination of the effective structure that is consistent with experiment for this nanophotonic system.

Table 1. Simulated and Experimental RET rates

Position of fluorophores	Interparticle gap (nm)	Simulation (ns^{-1})		Experiment (ns^{-1})	
		With NPs	Without NPs	With NPs	Without NPs
Vertical	14	2.88	2.19	6.3	1.3
	6	2.28			
	4	3.82			
Horizontal	10	4.83			
	8	8.59			
	6	32.79			
Diagonal	4	7.53			

CONCLUSIONS

The effect of a metal sphere (gold and silver) on the RET rate between two fluorophores was investigated under the point dipole approximation with an emphasis on geometrical parameters. It was identified that the highest PEFs arise from positioning the fluorophores on the opposite sides of the NP, as close to the NP as possible without quenching, and using a larger NP (>50 nm). Changing dipole orientations drastically alters the PEF profile such that RET was suppressed by the presence of the NP when the dipoles were tangentially oriented relative to the NP surface. The concept of a consistent D-A distance (20 nm) that leads to maximally suppressed RET was discovered. We also showed that after factoring in the enhancement of absorption by the

nanoparticle, the AF rate follows a similar trend as RET but can lead to enhancements even when RET is suppressed. A quasistatic analysis using a Green function revealed that the higher-order multipole contributions to PC-RET are greater for smaller fluorophore–NP distances and larger NPs. Analysis of an experiment demonstrated how the dependence of the RET rate on geometry of a nanophotonic system plays a crucial role in relating rate information to possible system structure.

AUTHOR INFORMATION

Corresponding Author

*E-mail: g-schatz@northwestern.edu (G.C.S.).

ORCID

Yeonjun Jeong: 0000-0001-7144-8775

George C. Schatz: 0000-0001-5837-4740

Notes

The authors declare no competing financial interest.

ASSOCIATED CONTENT

Supporting Information. The Supporting Information is available free of charge free of charge on the ACS Publications website at DOI:

PEF of a single D-A pair near a silver sphere with various relative positions of the donor and the acceptor with respect to each other and the sphere and the orientation of the donor and the acceptor, arc length formed by the D-A pair at the minimum PEF point with various gold and

silver sphere size, and geometry setup and results of a simulation of RET rate of a D-A pair between a gold dimer (PDF)

ACKNOWLEDGMENT

This work was supported by U.S. National Science Foundation under grant number CHE-1760537. We thank Wendu Ding for valuable discussions. Wendu Ding and Charles W. Heaps contributed to the computer code used for the Mie theory calculations.

REFERENCES

1. Henzie, J.; Lee, J.; Lee, M. H.; Hasan, W.; Odom, T. W., Nanofabrication of Plasmonic Structures. *Annual Review of Physical Chemistry* **2009**, *60*, 147-165.
2. Biswas, A.; Bayer, I. S.; Biris, A. S.; Wang, T.; Dervishi, E.; Faupel, F., Advances in Top–Down and Bottom–up Surface Nanofabrication: Techniques, Applications & Future Prospects. *Advances in Colloid and Interface Science* **2012**, *170*, 2-27.
3. Wang, D.; Wang, W.; Knudson, M. P.; Schatz, G. C.; Odom, T. W., Structural Engineering in Plasmon Nanolasers. *Chemical Reviews* **2018**, *118*, 2865-2881.
4. Alix-Panabières, C.; Pantel, K., Here Comes the Spaser. *Nature Materials* **2017**, *16*, 790.
5. Galanzha, E. I., et al., Spaser as a Biological Probe. *Nature Communications* **2017**, *8*, 15528.
6. Wang, S., et al., Plasmonic Copper Sulfide Nanocrystals Exhibiting near-Infrared Photothermal and Photodynamic Therapeutic Effects. *ACS Nano* **2015**, *9*, 1788-1800.
7. Aouani, H.; Schön, P.; Brasselet, S.; Rigneault, H.; Wenger, J., Two-Photon Fluorescence Correlation Spectroscopy with High Count Rates and Low Background Using Dielectric Microspheres. *Biomed. Opt. Express* **2010**, *1*, 1075-1083.
8. Aouani, H.; Itzhakov, S.; Gachet, D.; Devaux, E.; Ebbesen, T. W.; Rigneault, H.; Oron, D.; Wenger, J., Colloidal Quantum Dots as Probes of Excitation Field Enhancement in Photonic Antennas. *ACS Nano* **2010**, *4*, 4571-4578.
9. Lakowicz, J. R.; Fu, Y., Modification of Single Molecule Fluorescence near Metallic Nanostructures. *Laser & Photonics Reviews* **2009**, *3*, 221-232.
10. Wenger, J.; Rigneault, H., Photonic Methods to Enhance Fluorescence Correlation Spectroscopy and Single Molecule Fluorescence Detection. *Int J Mol Sci* **2010**, *11*, 206-221.
11. Gérard, D.; Devilez, A.; Aouani, H.; Stout, B.; Bonod, N.; Wenger, J.; Popov, E.; Rigneault, H., Efficient Excitation and Collection of Single-Molecule Fluorescence Close to a Dielectric Microsphere. *J. Opt. Soc. Am. B* **2009**, *26*, 1473-1478.
12. Schuck, P. J.; Fromm, D. P.; Moerner, W. E.; Sundaramurthy, A.; Kino, G. In *Gold Bowtie Nanoantennas: Improving the Mismatch between Light and Nanoscale Objects*, Conference on Lasers and Electro-Optics/Quantum Electronics and Laser Science and Photonic Applications Systems Technologies, Baltimore, Maryland, 2005/05/22; Optical Society of America: Baltimore, Maryland, 2005; p QMH1.

13. Mühlschlegel, P.; Eisler, H. J.; Martin, O. J. F.; Hecht, B.; Pohl, D. W., Resonant Optical Antennas. *Science* **2005**, *308*, 1607.
14. Djaker, N.; Hostein, R.; Devaux, E.; Ebbesen, T. W.; Rigneault, H.; Wenger, J., Surface Enhanced Raman Scattering on a Single Nanometric Aperture. *The Journal of Physical Chemistry C* **2010**, *114*, 16250-16256.
15. Ko, H.; Singamaneni, S.; Tsukruk, V. V., Nanostructured Surfaces and Assemblies as Sers Media. *Small* **2008**, *4*, 1576-1599.
16. Schön, P.; Bonod, N.; Devaux, E.; Wenger, J.; Rigneault, H.; Ebbesen, T. W.; Brasselet, S., Enhanced Second-Harmonic Generation from Individual Metallic Nanoapertures. *Opt. Lett.* **2010**, *35*, 4063-4065.
17. Andrew, P.; Barnes, W. L., Förster Energy Transfer in an Optical Microcavity. *Science* **2000**, *290*, 785.
18. Bidault, S.; Devilez, A.; Ghenuche, P.; Stout, B.; Bonod, N.; Wenger, J., Competition between Förster Resonance Energy Transfer and Donor Photodynamics in Plasmonic Dimer Nanoantennas. *ACS Photonics* **2016**, *3*, 895-903.
19. Ghenuche, P.; de Torres, J.; Moparthi, S. B.; Grigoriev, V.; Wenger, J., Nanophotonic Enhancement of the Förster Resonance Energy-Transfer Rate with Single Nanoapertures. *Nano Letters* **2014**, *14*, 4707-4714.
20. Martín-Cano, D.; Martín-Moreno, L.; García-Vidal, F. J.; Moreno, E., Resonance Energy Transfer and Superradiance Mediated by Plasmonic Nanowaveguides. *Nano Letters* **2010**, *10*, 3129-3134.
21. Baibakov, M.; Patra, S.; Claude, J.-B.; Moreau, A.; Lumeau, J.; Wenger, J., Extending Single-Molecule Förster Resonance Energy Transfer (Fret) Range Beyond 10 Nanometers in Zero-Mode Waveguides. *ACS Nano* **2019**, *13*, 8469-8480.
22. Rustomji, K.; Dubois, M.; Kuhlmey, B.; de Sterke, C. M.; Enoch, S.; Abdeddaim, R.; Wenger, J., Direct Imaging of the Energy-Transfer Enhancement between Two Dipoles in a Photonic Cavity. *Physical Review X* **2019**, *9*, 011041.
23. Choi, Y.; Park, Y.; Kang, T.; Lee, L. P., Selective and Sensitive Detection of Metal Ions by Plasmonic Resonance Energy Transfer-Based Nanospectroscopy. *Nature Nanotechnology* **2009**, *4*, 742.
24. Novotny, L.; Hecht, B., *Principles of Nano-Optics*; Cambridge University Press: Cambridge, 2006.
25. Ghenuche, P.; Mivelle, M.; de Torres, J.; Moparthi, S. B.; Rigneault, H.; Van Hulst, N. F.; García-Parajó, M. F.; Wenger, J., Matching Nanoantenna Field Confinement to Fret Distances Enhances Förster Energy Transfer Rates. *Nano Letters* **2015**, *15*, 6193-6201.
26. de Torres, J.; Mivelle, M.; Moparthi, S. B.; Rigneault, H.; Van Hulst, N. F.; García-Parajó, M. F.; Margeat, E.; Wenger, J., Plasmonic Nanoantennas Enable Forbidden Förster Dipole–Dipole Energy Transfer and Enhance the Fret Efficiency. *Nano Letters* **2016**, *16*, 6222-6230.
27. de Torres, J.; Ferrand, P.; Colas des Francs, G.; Wenger, J., Coupling Emitters and Silver Nanowires to Achieve Long-Range Plasmon-Mediated Fluorescence Energy Transfer. *ACS Nano* **2016**, *10*, 3968-3976.
28. Zhang, X.; Marocico, C. A.; Lunz, M.; Gerard, V. A.; Gun'ko, Y. K.; Lesnyak, V.; Gaponik, N.; Susha, A. S.; Rogach, A. L.; Bradley, A. L., Experimental and Theoretical Investigation of the Distance Dependence of Localized Surface Plasmon Coupled Förster Resonance Energy Transfer. *ACS Nano* **2014**, *8*, 1273-1283.

29. Bujak, Ł.; Ishii, T.; Sharma, D. K.; Hirata, S.; Vacha, M., Selective Turn-on and Modulation of Resonant Energy Transfer in Single Plasmonic Hybrid Nanostructures. *Nanoscale* **2017**, *9*, 1511-1519.
30. Bohlen, J.; Cuartero-González, Á.; Pibiri, E.; Ruhlandt, D.; Fernández-Domínguez, A. I.; Tinnefeld, P.; Acuna, G. P., Plasmon-Assisted Förster Resonance Energy Transfer at the Single-Molecule Level in the Moderate Quenching Regime. *Nanoscale* **2019**, *11*, 7674-7681.
31. Anderson, N. T.; Ren, S.; Chao, J.; Dinolfo, P. H.; Wang, X., Exploiting Plasmon-Mediated Energy Transfer to Enhance End-to-End Efficiency in a DNA Origami Energy Transfer Array. *ACS Applied Nano Materials* **2019**, *2*, 5563-5572.
32. Förster, T., Zwischenmolekulare Energiewanderung Und Fluoreszenz. *Annalen der Physik* **1948**, *437*, 55-75.
33. Förster, T., Energiewanderung Und Fluoreszenz. *Naturwissenschaften* **1946**, *33*, 166-175.
34. Anger, P.; Bharadwaj, P.; Novotny, L., Enhancement and Quenching of Single-Molecule Fluorescence. *Physical Review Letters* **2006**, *96*, 113002.
35. Craig, D. P.; Thirunamachandran, T., *Molecular Quantum Electrodynamics: An Introduction to Radiation-Molecule Interactions*; Dover Publications: Mineola, NY, 1998.
36. Power, E. A.; Thirunamachandran, T., Quantum Electrodynamics with Nonrelativistic Sources. Iii. Intermolecular Interactions. *Physical Review A* **1983**, *28*, 2671-2675.
37. Daniels, G. J.; Jenkins, R. D.; Bradshaw, D. S.; Andrews, D. L., Resonance Energy Transfer: The Unified Theory Revisited. *The Journal of Chemical Physics* **2003**, *119*, 2264-2274.
38. Andrews, D. L., A Unified Theory of Radiative and Radiationless Molecular Energy Transfer. *Chemical Physics* **1989**, *135*, 195-201.
39. Andrews, D. L.; Sherborne, B. S., Resonant Excitation Transfer: A Quantum Electrodynamical Study. *The Journal of Chemical Physics* **1987**, *86*, 4011-4017.
40. Andrews, D. L.; Juzeliūnas, G., Intermolecular Energy Transfer: Retardation Effects. *The Journal of Chemical Physics* **1992**, *96*, 6606-6612.
41. Jenkins, R. D.; Daniels, G. J.; Andrews, D. L., Quantum Pathways for Resonance Energy Transfer. *The Journal of Chemical Physics* **2004**, *120*, 11442-11448.
42. Grinter, R.; Jones, G. A., Resonance Energy Transfer: The Unified Theory Via Vector Spherical Harmonics. *The Journal of Chemical Physics* **2016**, *145*, 074107.
43. Juzeliūnas, G.; Andrews, D. L., Quantum Electrodynamics of Resonant Energy Transfer in Condensed Matter. *Physical Review B* **1994**, *49*, 8751-8763.
44. Hua, X. M.; Gersten, J. I.; Nitzan, A., Theory of Energy Transfer between Molecules near Solid State Particles. *The Journal of Chemical Physics* **1985**, *83*, 3650-3659.
45. Jones, G. A.; Bradshaw, D. S., Resonance Energy Transfer: From Fundamental Theory to Recent Applications. *Frontiers in Physics* **2019**, *7*, 100.
46. Dung, H. T.; Knöll, L.; Welsch, D.-G., Intermolecular Energy Transfer in the Presence of Dispersing and Absorbing Media. *Physical Review A* **2002**, *65*, 043813.
47. Poudel, A.; Chen, X.; Ratner, M. A., Enhancement of Resonant Energy Transfer Due to an Evanescent Wave from the Metal. *The Journal of Physical Chemistry Letters* **2016**, *7*, 955-960.
48. Ding, W.; Hsu, L.-Y.; Schatz, G. C., Plasmon-Coupled Resonance Energy Transfer: A Real-Time Electrodynamics Approach. *The Journal of Chemical Physics* **2017**, *146*, 064109.
49. Hsu, L.-Y.; Ding, W.; Schatz, G. C., Plasmon-Coupled Resonance Energy Transfer. *The Journal of Physical Chemistry Letters* **2017**, *8*, 2357-2367.

50. Ringler, M.; Schwemer, A.; Wunderlich, M.; Nichtl, A.; Kürzinger, K.; Klar, T. A.; Feldmann, J., Shaping Emission Spectra of Fluorescent Molecules with Single Plasmonic Nanoresonators. *Physical Review Letters* **2008**, *100*, 203002.
51. Ding, W.; Hsu, L.-Y.; Heaps, C. W.; Schatz, G. C., Plasmon-Coupled Resonance Energy Transfer Ii: Exploring the Peaks and Dips in the Electromagnetic Coupling Factor. *The Journal of Physical Chemistry C* **2018**, *122*, 22650-22659.
52. Delga, A.; Feist, J.; Bravo-Abad, J.; Garcia-Vidal, F. J., Quantum Emitters near a Metal Nanoparticle: Strong Coupling and Quenching. *Physical Review Letters* **2014**, *112*, 253601.
53. Wu, J.-S.; Lin, Y.-C.; Sheu, Y.-L.; Hsu, L.-Y., Characteristic Distance of Resonance Energy Transfer Coupled with Surface Plasmon Polaritons. *The Journal of Physical Chemistry Letters* **2018**, *9*, 7032-7039.
54. Nasiri Avanaki, K.; Ding, W.; Schatz, G. C., Resonance Energy Transfer in Arbitrary Media: Beyond the Point Dipole Approximation. *The Journal of Physical Chemistry C* **2018**, *122*, 29445-29456.
55. Craig, D. P.; Thirunamachandran, T., Chiral Discrimination in Molecular Excitation Transfer. *The Journal of Chemical Physics* **1998**, *109*, 1259-1263.
56. Jackson, J. D., *Classical Electrodynamics*; New York: Wiley, 1999.
57. Mie, G., Articles on the Optical Characteristics of Turbid Tubes, Especially Colloidal Metal Solutions. *Annals of Physics* **1908**, *25*.
58. Bohren, C. F.; Huffman, D. R., *Absorption and Scaterring of Light by Small Particles*; John Wiley and Sons, 1983.
59. Le Ru, E. C.; Etchegoin, P. G., *Principles of Surface-Enhanced Raman Spectroscopy*; Elsevier, 2009.
60. Heaps, C. W.; Schatz, G. C., Modeling Super-Resolution Sers Using a T-Matrix Method to Elucidate Molecule-Nanoparticle Coupling and the Origins of Localization Errors. *The Journal of chemical physics* **2017**, *146*, 224201-224201.
61. Ausman, L. K.; Schatz, G. C., Whispering-Gallery Mode Resonators: Surface Enhanced Raman Scattering without Plasmons. *The Journal of Chemical Physics* **2008**, *129*, 054704.
62. Mackowski, D. W., Analysis of Radiative Scattering for Multiple Sphere Configurations. *Proceedings of the Royal Society of London. Series A: Mathematical and Physical Sciences* **1991**, *433*, 599-614.
63. Mackowski, D. W., Calculation of Total Cross Sections of Multiple-Sphere Clusters. *J. Opt. Soc. Am. A* **1994**, *11*, 2851-2861.
64. Schwinger, J.; Deraad Jr., L. L.; Milton, K.; Tsai, W., *Classical Electrodynamics*; Perseus Books: Reading, 1998.
65. Jeong, Y.; Schatz, G. C., Plasmon-Coupled Resonance Energy Transfer and Photocatalysis: Theory and Application. In *Springer Handbook of Inorganic Photochemistry*, Springer Nature: 2020, in press.
66. Schatz, G. C.; Ratner, M. A., *Quantum Mechanics in Chemistry*; Dover: Englewood Cliffs, N.J., 1993.
67. Zeman, E. J.; Carron, K. T.; Schatz, G. C.; Van Duyne, R. P., A Surface Enhanced Resonance Raman Study of Cobalt Phthalocyanine on Rough Ag Films: Theory and Experiment. *The Journal of Chemical Physics* **1987**, *87*, 4189-4200.
68. Kelly, K. L.; Coronado, E.; Zhao, L. L.; Schatz, G. C., The Optical Properties of Metal Nanoparticles: The Influence of Size, Shape, and Dielectric Environment. *The Journal of Physical Chemistry B* **2003**, *107*, 668-677.

69. Manning, G. S., The Persistence Length of DNA Is Reached from the Persistence Length of Its Null Isomer through an Internal Electrostatic Stretching Force. *Biophys J* **2006**, *91*, 3607-3616.

TOC Graphic